



# Hydrothermal synthesis of Siliceous Beta Zeolite by an inorganic cation-driven strategy and its crystallization mechanism

Dongxia Luo<sup>a,b,1</sup>, Quanyi Wang<sup>a,1</sup>, Dong Fan<sup>a</sup>, Miao Yang<sup>a</sup>, Benhan Fan<sup>a,c</sup>, Kaipeng Cao<sup>a,c</sup>, Shutao Xu<sup>a</sup>, Peng Tian<sup>a,c,\*</sup>, Zhongmin Liu<sup>a,c,\*\*</sup>

<sup>a</sup> National Engineering Laboratory for Methanol to Olefins, Dalian National Laboratory for Clean Energy, Dalian Institute of Chemical Physics, Chinese Academy of Sciences, Dalian, 116023, China

<sup>b</sup> Green Catalysis Center, And College of Chemistry, Zhengzhou University, Zhengzhou, 450001, China

<sup>c</sup> University of Chinese Academy of Sciences, Beijing, 100049, China

## ARTICLE INFO

### Keywords:

Siliceous beta  
Fluoride-free hydrothermal synthesis  
Inorganic cation-driven  
Crystallization mechanism  
VOCs adsorption

## ABSTRACT

Siliceous Beta zeolite and its metal-containing counterparts are effective adsorption and catalysis materials. To develop facile and efficient synthesis strategy would facilitate their large-scale production and application. Herein, we report the fluoride-free hydrothermal synthesis of siliceous Beta achieved by an inorganic cation-driven strategy. It is found that the types of inorganic cations are more critical than anions in determining the product phase. Inorganic cations with smaller sizes (such as  $\text{Li}^+$ ,  $\text{Na}^+$  and  $\text{Mg}^{2+}$ ) facilitate the synthesis of siliceous Beta, while the larger ones (such as  $\text{K}^+$ ,  $\text{Ca}^{2+}$  and  $\text{NH}_4^+$ ) tend to give rise to impurity or amorphous materials. Crystallization mechanism investigation based on the  $\text{Na}^+$ -added system revealed that inorganic cations can effectively promote the fast polymerization of  $\text{SiO}_2$  colloids at the initial stage. The crystallization occurs on the polymerized composites, yielding siliceous Beta with high solid yield. The resultant material is well characterized, which possesses few framework defects, high hydrophobicity and large adsorption uptake for toluene (one of the common volatile organic compounds). Breakthrough experiments further evidence the dynamic toluene adsorption capacity of the material is 24% higher than that of siliceous Beta synthesized by fluoride route.

## 1. Introduction

Zeolites contribute to the building of modern energy, chemical and environmental industries, which have been widely employed as the catalysts and adsorbents for the numerous processes [1–5]. Besides the prominent roles in various chemical processes, the anonymous contributions from zeolites in adsorbents receive growing spotlights, given the increasingly stringent regulations on energy and environmental standards. The most early and well-known zeolite-based adsorbents are the desiccating adsorbents associated with LTA (A) and FAU (X) zeolites, which reach the historical and ongoing milestone regarding their applications in world wide. The capability and capacity of zeolite-based adsorbents depend on their topology and Si/Al ratios, the latter of

which reflects their affinity to the inorganic/organic guest adsorbates. As the consequence, the Al-rich, i.e. low Si/Al ratios, zeolites are popular for the relatively polar guest adsorbates, whereas Al-deficient zeolites prefer less polar ones [4,6–9].

Volatile organic compounds (VOCs) are pervasive in our daily life, which is toxic for human health and environments. Zeolite Beta with three-dimensional (3D) 12-ring large pores is among the most promising candidates for the abatement of VOCs, especially for bulky VOCs [4, 10–14]. Hydrophobic all-silica Beta zeolite has shown excellent performance in the competitive adsorption of organic-water mixtures in comparison with other zeolites [4,10,11,15]. Very recently, siliceous Beta was further reported to be highly selective for the removal of perfluorinated contaminants, even in the presence of organic

\* Corresponding author. National Engineering Laboratory for Methanol to Olefins, Dalian National Laboratory for Clean Energy, Dalian Institute of Chemical Physics, Chinese Academy of Sciences, Dalian, 116023, China.

\*\* Corresponding author. National Engineering Laboratory for Methanol to Olefins, Dalian National Laboratory for Clean Energy, Dalian Institute of Chemical Physics, Chinese Academy of Sciences, Dalian, 116023, China.

E-mail addresses: [tianpeng@dicp.ac.cn](mailto:tianpeng@dicp.ac.cn) (P. Tian), [liuzm@dicp.ac.cn](mailto:liuzm@dicp.ac.cn) (Z. Liu).

<sup>1</sup> These authors contributed equally to this work.

competitors [16]. The lack of silanol defects in the zeolite framework was revealed to be important for the high adsorption affinity and high saturation capacity.

Conventionally, zeolite Beta is hydrothermally synthesized using tetraethylammonium hydroxide (TEAOH) as an organic-structure directing agent (OSDA), and the product Si/Al ratio (SAR) is lower than 100 [17,18]. Given the importance and application potentials of siliceous Beta zeolite, great efforts have been dedicated to breaking the limit. Post-synthesis dealumination method offers an indirect alternative to prepare siliceous Beta. However, loss of crystallinity cannot be avoided during the acid treatment, yielding a product with abundant internal defects [19,20]. This is unfavorable for the material's adsorption performance as industrial gases always contain both VOCs and water vapor. van der Waals et al. [21] first reported the synthesis of all-silica Beta by using commercially unavailable dibenzylidimethylammonium cation as OSDA under the assistance of Beta seeds. The existence of Si-OH defects ( $Q^3/(Q^3+Q^4) = 0.16$ ) revealed by  $^{29}\text{Si}$  MAS NMR implied its poor hydrophobicity. Subsequently, Cambor et al. [22] synthesized siliceous Beta and Ti-Beta by using tetraethylorthosilicate (TEOS) as Si source under the addition of  $\text{H}_2\text{O}_2$  and seeds after a crystallization at  $140\text{ }^\circ\text{C}$  for 14 days. Comparatively, fluoride-assisted synthesis provides an effective way to achieve defects-free large Beta crystals. Based on fluoride-assisted method, some novel OSDAs for the synthesis of siliceous Beta were also discovered [23–26]. Unfortunately, the use of highly corrosive and toxic fluoride in the synthetic system restricted its large-scale production due to pollution and safety problems [27]. Recently, Fan et al. [28] reported the synthesis of siliceous zeolites by dry gel conversion (DGC). They proposed that the charge-balancing interactions between the inorganic cation, OSDA, and Si-O<sup>-</sup> defects play crucial role for the synthesis. In addition, interzeolite transformation method was also developed to synthesize siliceous Beta by using MWW zeolite (ITQ-1) as starting precursor. The  $\text{H}_2\text{O}$  dosage is controlled at very low level ( $\text{H}_2\text{O}/\text{SiO}_2 = 1$ ) to reach satisfied crystallinity and yield [15]. However, the above DGC strategy and phase transformation route are hard to be scaled up due to the difficulty in mass and heat transfer.

To develop efficient and fluoride-free hydrothermal synthesis strategy for siliceous Beta zeolite is thus highly desirable, which would facilitate its large-scale synthesis and promote its industrial application. Moreover, metal<sup>IV</sup>-containing siliceous Beta zeolites such as Sn-Beta [29–32], Zr-Beta [32,33] and Ti-Beta [22,34,35] are important Lewis acid catalyst effective for many redox reactions. The development of novel/facile synthetic strategy for siliceous Beta would also facilitate the synthesis and industrial application of these metal<sup>IV</sup>-containing Beta materials.

Herein, with the understanding of zeolites formation and colloid chemistry, an inorganic cation-driven polymerization strategy is developed to realize the efficient hydrothermal synthesis of siliceous Beta. All the sources were those conventionally employed for the large-scale production of zeolites. The zeolite formation mechanism was studied systematically and the intrinsic role of inorganic cation on the synthesis was proposed. The hydrophobicity and VOCs adsorption performance of the obtained material were investigated and compared with the ones synthesized by fluoride route and by post-synthesis dealumination.

## 2. Experimental

### 2.1. Materials

The chemical reactants used for zeolite synthesis: tetraethylammonium hydroxide (TEAOH, 35 wt%), tetraethylammonium chloride (TEACl, 99 wt%), tetramethylammonium chloride (TMACl, 99.9 wt%), silica gel (99 wt%), silica sol (27.5 wt%), fumed silica (99 wt%), tetraethyl orthosilicate (TEOS, 99 wt%), sodium hydroxide (NaOH, 99.9 wt%), lithium chloride (LiCl, 97 wt%), sodium chloride (NaCl, 99.5 wt%), sodium bromide (NaBr, 99 wt%), sodium nitrate ( $\text{NaNO}_3$ , 99 wt%),

sodium sulfate ( $\text{Na}_2\text{SO}_4$ , 99 wt%), potassium bromide (KBr, 99 wt%), potassium chloride (KCl, 99.5 wt%), magnesium chloride hexahydrate ( $\text{MgCl}_2 \cdot 6\text{H}_2\text{O}$ , 98 wt%), calcium chloride ( $\text{CaCl}_2$ , 96 wt%), ammonium chloride ( $\text{NH}_4\text{Cl}$ , 99 wt%), hydrofluoric acid (HF, 40 wt%), aluminium isopropoxide (24.7 wt%), nitric acid ( $\text{HNO}_3$ , 65 wt%) ammonium nitrate ( $\text{NH}_4\text{NO}_3$ , 99.5 wt%), toluene (99 wt%). All of them were commercial reagents and used as received.

### 2.2. Fluoride-free hydrothermal synthesis of siliceous Beta zeolite

The detailed gel compositions for the fluoride-free hydrothermal synthesis of siliceous Beta zeolite were listed in Table 1. The typical synthesis procedure can be described as follows: TEAOH solution was first added into deionized water, followed by the addition of TEACl and NaCl. The mixture was stirred for about 10 min to obtain a clear solution. Fumed silica was then added into the above solution in three equal lots under stirring. After stirring the gel at room temperature for 12 h, siliceous Beta seeds were added if required. After a further stirring for 12 h, the final gel was transferred to a stainless-steel autoclave and heated in an oven maintained at  $140\text{ }^\circ\text{C}$  for 4 d. The as-made sample was recovered by centrifugation, washed with deionized water for 3 times and dried at  $120\text{ }^\circ\text{C}$ .

As the existence of  $\text{Na}^+$  cation in the as-made sample may cause the structural collapse during the calcination process,  $\text{NH}_4^+$  exchange was conducted to remove the metal cations in the as-made sample [36]. 1 g of the sample was mixed with 50 g of 1 mol/L  $\text{NH}_4\text{Cl}$  solution and stirred at  $80\text{ }^\circ\text{C}$  for 1 h. The solid was recovered by centrifugation, and this process was repeated two times. The resultant sample was dried at  $120\text{ }^\circ\text{C}$  and calcined in air at  $600\text{ }^\circ\text{C}$  for 5 h to remove the organics.

In all experiments, the oven was heated to  $140\text{ }^\circ\text{C}$  in 1 h. For the investigation of crystallization process, time zero was recorded once the oven temperature reached  $140\text{ }^\circ\text{C}$ .

### 2.3. Preparation of Beta nanoseeds

NaOH was first dissolved in TEAOH solution, followed by the gradual addition of fumed silica. After the silica dissolved, aluminium isopropoxide was added into the solution, which form a gel with molar composition of  $25\text{SiO}_2 : 0.25\text{Al}_2\text{O}_3 : 9\text{TEAOH} : 0.35\text{Na}_2\text{O} : 331\text{H}_2\text{O}$  [28]. This mixture was stirred at room temperature for 1 d followed by heating in a stainless-steel autoclave at  $120\text{ }^\circ\text{C}$  for 3 d. The product was washed with deionized water, calcined at  $600\text{ }^\circ\text{C}$  for 5 h and dealuminated by treatment with concentrated  $\text{HNO}_3$  at  $80\text{ }^\circ\text{C}$  for 24 h. This

**Table 1**  
Synthesis conditions and products of siliceous Beta zeolite.

Sample <sup>a</sup>	Gel composition	Product		
		Yield <sup>b</sup> (wt %)	Phase	Si/Na <sup>c</sup> (mole)
1	$1\text{SiO}_2 : 0.35\text{TEAOH} : 7\text{H}_2\text{O}$	–	Clear liquid	–
2	$1\text{SiO}_2 : 0.35\text{TEAOH} : 7\text{H}_2\text{O}$	9.3	Beta	–
3	$1\text{SiO}_2 : 0.35\text{TEAOH} : 0.20\text{NaCl} : 7\text{H}_2\text{O}$	62.9	Beta	21
4	$1\text{SiO}_2 : 0.25\text{TEAOH} : 0.1\text{TEACl} : 0.05\text{NaCl} : 7\text{H}_2\text{O}$	42.0	Beta	50
5	$1\text{SiO}_2 : 0.25\text{TEAOH} : 0.1\text{TEACl} : 0.10\text{NaCl} : 7\text{H}_2\text{O}$	81.6	Beta	28
6	$1\text{SiO}_2 : 0.25\text{TEAOH} : 0.1\text{TEACl} : 0.20\text{NaCl} : 7\text{H}_2\text{O}$	88.6	Beta + ZSM-5+Amor.	10
7	$1\text{SiO}_2 : 0.20\text{TEAOH} : 0.15\text{TEACl} : 0.10\text{NaCl} : 7\text{H}_2\text{O}$	87.4	Beta + ZSM-5+Amor.	19

<sup>a</sup> All the syntheses were carried out at  $140\text{ }^\circ\text{C}$  for 4 days with the addition of 10 wt% seeds except sample 1 (without seeds addition).

<sup>b</sup> Calculated on the basis of  $\text{SiO}_2$  mass: solid yield =  $\text{SiO}_2 \text{ product} / (\text{SiO}_2 \text{ source} + \text{SiO}_2 \text{ seeds})$ . The  $\text{SiO}_2 \text{ product}$  does not include the OSDA weight.

<sup>c</sup> Si/Na ratio of the as-made products.

treatment was capable to extensively remove alumina in the parent zeolite. After calcination at 600 °C for 5 h, the product was collected by centrifugation and washed thoroughly with deionized water.

#### 2.4. Preparation of reference samples

Two reference samples named Ref<sub>deAl</sub> and Ref<sub>F</sub> were prepared for comparison. Ref<sub>deAl</sub> was obtained by post-synthesis dealumination of aluminosilicate Beta. The detailed procedure is the same as that of Beta nanoseeds described above. Ref<sub>F</sub> was synthesized by a fluoride-assisted route. Its synthesis procedure is as follows: TEOAH solution was added to a plastic beaker, followed by the addition of fumed silica in three equal lots while stirring. After stirring for 2h, HF solution was fast added into the mixture. The redundant water was evaporated at 60 °C to obtain the final gel with a molar composition of 1.0SiO<sub>2</sub>: 0.5TEAOH: 0.6HF: 3H<sub>2</sub>O [37]. This mixture was transferred into a stainless-steel autoclave and heated at 160 °C for 1 d. The solid was recovered by centrifugation, washed with deionized water, dried at 120 °C and finally calcined at 600 °C for 5 h.

#### 2.5. Characterization

X-ray diffraction (XRD) patterns of the samples were collected on a PANalytical X'Pert PRO X-ray diffractometer using Cu K $\alpha$  radiation ( $\lambda = 1.5418 \text{ \AA}$ ) at 40 mA and 40 kV. The inorganic elemental compositions were determined using a Philips Magix-601 X-ray fluorescence (XRF) spectrometer. Scanning electron microscopy (SEM) images were obtained for morphological investigation using a Hitachi SU8020 scanning electron microscope. N<sub>2</sub> adsorption and desorption experiments were performed on an ASAP 2020 gas adsorption analyzer (Micromeritics) at -196 °C. The sample was pre-treated under vacuum at 350 °C for 4 h before the test. The solid-state nuclear magnetic resonances (NMR) were measured on a Bruker Avance III 600 spectrometer equipped with a 14.1 T wide-bore magnet using a 4 mm WVT double resonances MAS probe. <sup>29</sup>Si MAS NMR utilized high energy proton decoupling to collect signals with the spinning rate of 8 kHz. The total number of scans was 1000 with 10 s cycle delays. The chemical shifts of Kaolinite at -91.5 ppm were used as reference. A TA SDT Q-600 analyzer was used for thermogravimetry analysis (TGA) under 50 mL/min of air flow and the heating rate was set at 10 °C/min. The sample was packed at about 10 mg and tested from room temperature to 900 °C. The FTIR spectra were recorded in the range of 4000–900 cm<sup>-1</sup> on a Fourier transform infrared spectrometer (Brukers XF808-04) with a resolution of 4 cm<sup>-1</sup>. In order to remove the adsorbed water, the pellet was pretreated inside the IR cell at 450 °C in vacuum for 2 h before the measurement.

The water vapor adsorption isotherms of the samples were determined by ASAP 2020 physical adsorption apparatus of Micromeritics Company. Prior to the test, the samples (50 mg, 40–60 mesh) were degassed at 350 °C for 3 h. The toluene adsorption on zeolites was analyzed using Hiden Isochema IGA100 intelligent gravimetric analyzer. Before the test, the sample (100 mg, 40–60 mesh) was degassed at 350 °C for 1 h. The adsorption was carried out under the pulse pressure with a constant temperature of 25 °C and 33.8 mbar.

For the breakthrough experiment, 0.20 g of the calcined sample (40–60 mesh) was loaded in the stainless tube with internal diameter of 0.60 cm (bed height: ~2.2 cm). The sample was first purged with N<sub>2</sub> and heated to 600 °C for activation. The breakthrough temperature was controlled at 30 °C by circulating water bath. The adsorption was carried out with a mixture of toluene (1.87 kPa) and water vapor (0.87 kPa) using N<sub>2</sub> as carrying gas. The gas stream was analyzed by using a mass spectrometer.

### 3. Results and discussion

#### 3.1. Synthesis and characterization of siliceous Beta zeolite

Table 1 lists the detailed synthetic gel compositions and their effect on the product phases and yields. The corresponding XRD patterns of the products are displayed in Fig. S1. The hydrothermal syntheses of siliceous Beta started from a gel system with molar composition of 1SiO<sub>2</sub>: 0.35TEAOH: 7H<sub>2</sub>O. As shown in Table 1, no solid product was obtained simply based on this starting recipe after crystallization at 140 °C for 4 days. Upon the addition of siliceous Beta nanoseeds, the crystallization could be initiated but with low solid yield of 9.3%. Such a yield is close to the amount of added seeds. However, further adding NaCl into the system, the solid yield shows a remarkable increase to 62.9%, indicating the powerful effect of NaCl addition.

Aiming at the further improvement of solid yield, we tried to reduce the alkalinity of the gel system, given that previous works have evidenced that low alkalinity can decrease the solubility of siliceous species and help boost the solid yield of zeolites [9,38–40]. TEACl salt was thus added into the gel system to partially replace TEOAH, while fixing the total amount of OSDA cation (TEA<sup>+</sup>/SiO<sub>2</sub> = 0.35). It can be seen that under the gel composition of 1SiO<sub>2</sub>: 0.25TEAOH: 0.1TEACl: 0.1NaCl: 7H<sub>2</sub>O, the solid product can reach a yield as high as 81.6% with pure \*BEA phase (sample 5). Further decreasing the gel alkalinity to TEOAH/SiO<sub>2</sub> = 0.20, the solid yield shows a continuous increase to 87.4% (sample 7). Unfortunately, the resultant product was contaminated with impurity. In addition, the dosage of NaCl in the initial gel is also found to have a great effect on the purity and yield of solid products (samples 4–6). Lower NaCl addition shows weaker promotion on the increase of solid yield. High NaCl addition facilitates the improvement of solid yield, but may result in the formation of impurity. The optimized NaCl addition in the low-alkalinity gel system of samples 4–6 is at NaCl/SiO<sub>2</sub> = 0.1. The high solid yield and fluoride-free hydrothermal system of the present synthetic strategy imply that it would be favorable for the industrial production and application of siliceous Beta zeolite.

The characterization results of sample 5 are displayed in Fig. 1. The XRD pattern presents characteristic peaks of the \*BEA structure with both sharp and broad peaks, mainly comprised of the contribution of polymorphs A and B with stacking disorder [5,41,42]. The SEM image reveals that sample 5 has a truncated octahedron morphology with rough surface. The particle sizes are about 300–400 nm. The N<sub>2</sub> sorption isotherm of sample 5 gives a type IV isotherm with hysteresis loop in the range of P/P<sub>0</sub> = 0.40–0.95, showing the existence of mesopores which likely originate from the void space formed by the accumulation of adjacent nanocrystallines. The textural properties of the samples are shown in Table 2. The micropore surface area and micropore volume of sample 5 are 383 m<sup>2</sup> g<sup>-1</sup> and 0.19 cm<sup>3</sup> g<sup>-1</sup>, respectively, which are close to the previously reported values for zeolite Beta [43–45]. Thermogravimetry analysis displays that the as-made sample 5 contains an organic weight of about 22 wt%. The organics can be completely removed before 500 °C, which is much easier than that of aluminosilicate Beta and implies the relatively weak interactions between the TEA<sup>+</sup> and the siliceous framework.

It is noted that part of Na<sup>+</sup> cations is resided in the as-made product and its content shows a positive correlation with the initial dosage (Table 1). This is not unexpected as the involvement of Na<sup>+</sup> cations is necessary in order to compensate the negative charge of the framework ≡Si–O<sup>-</sup> defects, which are the residues following the formation of ≡Si–O<sup>-</sup> TEA<sup>+</sup> [46]. However, the existence of Na<sup>+</sup> cations may hinder the condensation of ≡Si–O<sup>-</sup> defects and lead to structural collapse during the high-temperature calcination process [47]. Therefore, NH<sub>4</sub><sup>+</sup>-ion exchange had been conducted for all the as-made Beta samples in the present work to remove Na<sup>+</sup> cations before calcination.

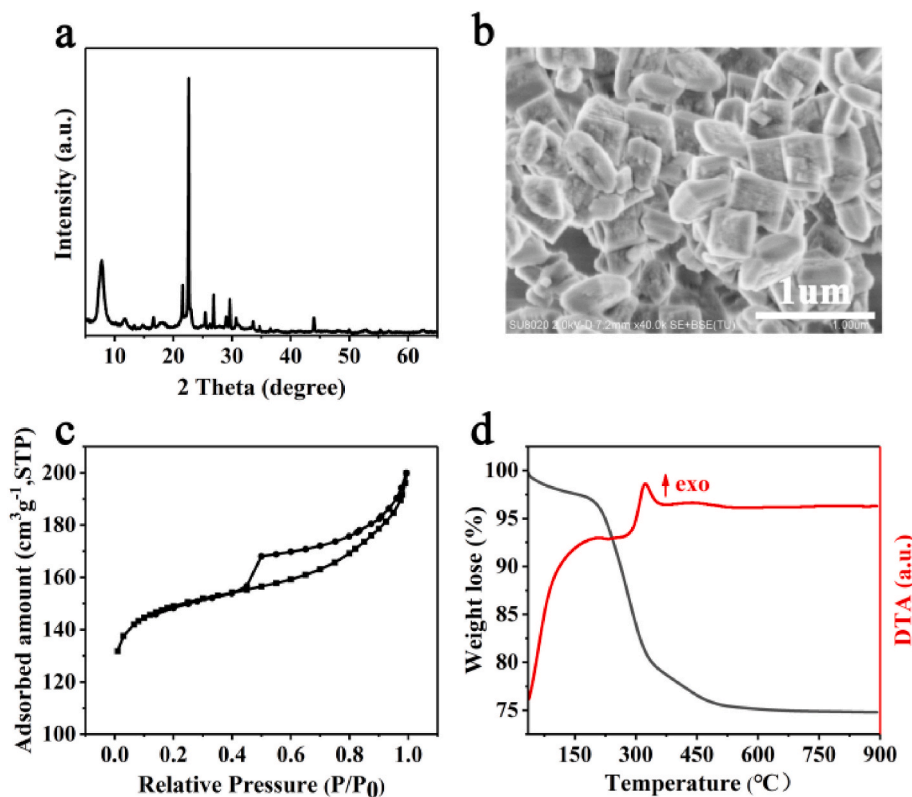


Fig. 1. XRD pattern (a), SEM image (b),  $N_2$  sorption isotherm (c) and TG-DTA curves (d) of sample 5. As-made sample for a, b and d; calcined sample for c.

Table 2

Textural properties of siliceous Beta zeolites.

Sample <sup>a</sup>	Pore volume <sup>b</sup> ( $\text{cm}^3 \text{g}^{-1}$ )			Surface area <sup>c</sup> ( $\text{m}^2 \text{g}^{-1}$ )		
	$V_{\text{total}}$	$V_{\text{micro}}$	$V_{\text{meso}}$	$S_{\text{total}}$	$S_{\text{micro}}$	$S_{\text{ext}}$
5	0.29	0.19	0.11	480	383	97
Ref <sub>F</sub>	0.27	0.18	0.09	452	369	82
Ref <sub>deAl</sub>	0.36	0.18	0.18	533	360	173

<sup>a</sup> Samples 5, Ref<sub>F</sub> and Ref<sub>deAl</sub> are obtained by calcination at 600 °C in air. Sample 5(720) is obtained by calcination of sample 5 at 720 °C in air.

<sup>b</sup>  $V_{\text{total}}$  is evaluated at  $P/P_0 = 0.97$ ;  $V_{\text{micro}}$ : t-plot micropore volume;  $V_{\text{meso}} = V_{\text{total}} - V_{\text{micro}}$ .

<sup>c</sup>  $S_{\text{total}}$ : BET surface area;  $S_{\text{micro}}$ : t-plot microporous surface area;  $S_{\text{ext}} = S_{\text{total}} - S_{\text{micro}}$ .

### 3.2. Effect of Si source and inorganic salt

The effect of Si source on the synthesis was investigated based on the recipe of sample 5 (Table S1). Clearly, except organic TEOS, silica sol, fumed silica and silica gel are all capable for the synthesis of siliceous Beta with high solid yield.

To understand the intrinsic reason of the NaCl addition for the enhancement of solid yield, more types of inorganic salts were explored for the synthetic system. As shown in Table 3 and Fig. S2, all the syntheses with the addition of inorganic salts (including  $\text{Na}^+$ ,  $\text{Li}^+$ ,  $\text{K}^+$ ,  $\text{Mg}^{2+}$ ,  $\text{Ca}^{2+}$  and  $\text{NH}_4^+$ ) are favorable for the increase of solid yield, despite their varied product phases. The types of cations are more critical than anions in determining the product phase. Synthetic systems with the addition of relatively small cations such as  $\text{Na}^+$ ,  $\text{Li}^+$  and  $\text{Mg}^{2+}$  give rise to pure Beta products, while the addition of larger  $\text{K}^+$ ,  $\text{Ca}^{2+}$  and  $\text{NH}_4^+$  result in the formation of impurity phases or amorphous materials. Among the cations,  $\text{Li}^+$  with the smallest size shows a superior effect in promoting the synthesis of siliceous Beta with high solid yield of 86.2%. These results suggest that the increase in solid yield promoted by

Table 3

The effect of the addition of inorganic salts on the synthesis of siliceous Beta.

Sample <sup>a</sup>	Salt addition	Product		
		Yield <sup>b</sup> (wt %)	Phase	Si/cation <sup>c</sup> (mole)
SA1	$m = 0$	17.5	Beta	–
SA2	$m = 0.2$ , LiCl	86.2	Beta	–
SA3	$m = 0.2$ , NaCl	53.6	Beta	22
SA4	$m = 0.2$ , NaBr	50.1	Beta	24
SA5	$m = 0.2$ , $\text{NaNO}_3$	43.1	Beta	26
SA6	$m = 0.1$ , $\text{Na}_2\text{SO}_4$	58.3	Beta	21
SA7	$m = 0.2$ , KBr	46.6	Beta + Impurity	10
SA8	$m = 0.2$ , KCl	52.4	Beta + Impurity	9
SA9	$m = 0.1$ , $\text{MgCl}_2$	51.9	Beta	20
SA10	$m = 0.1$ , $\text{CaCl}_2$	99.6	Beta + Amor.	11
SA11	$m = 0.2$ , $\text{NH}_4\text{Cl}$	77.5	Beta + Amor.	–

<sup>a</sup> All samples were synthesized with the initial gel of  $1\text{SiO}_2 \cdot 0.35\text{TEAOH}$ :  $m$  salt:  $8\text{H}_2\text{O}$  (10 wt% seeds) at 140 °C for 4 days. Silica gel as Si source.

<sup>b</sup> Calculated on the basis of  $\text{SiO}_2$  mass: solid yield =  $\text{SiO}_2 \text{ product} / (\text{SiO}_2 \text{ source} + \text{SiO}_2 \text{ seeds})$ . The  $\text{SiO}_2 \text{ product}$  does not include the OSDA weight.

<sup>c</sup> Si/cation ratio of the as-made products.

inorganic cations is indeed a common phenomenon, although some cations may interrupt/change the crystallization process and cause impurity or amorphous product.

### 3.3. Crystallization process and formation mechanism

The crystallization process of siliceous Beta zeolite is examined based on sample 5. Fig. 2 displays the evolution of XRD patterns, solid yields and Si/Na molar ratios of the products with different crystallization times. Fig. S3 presents the evolution of XRD patterns of siliceous Beta

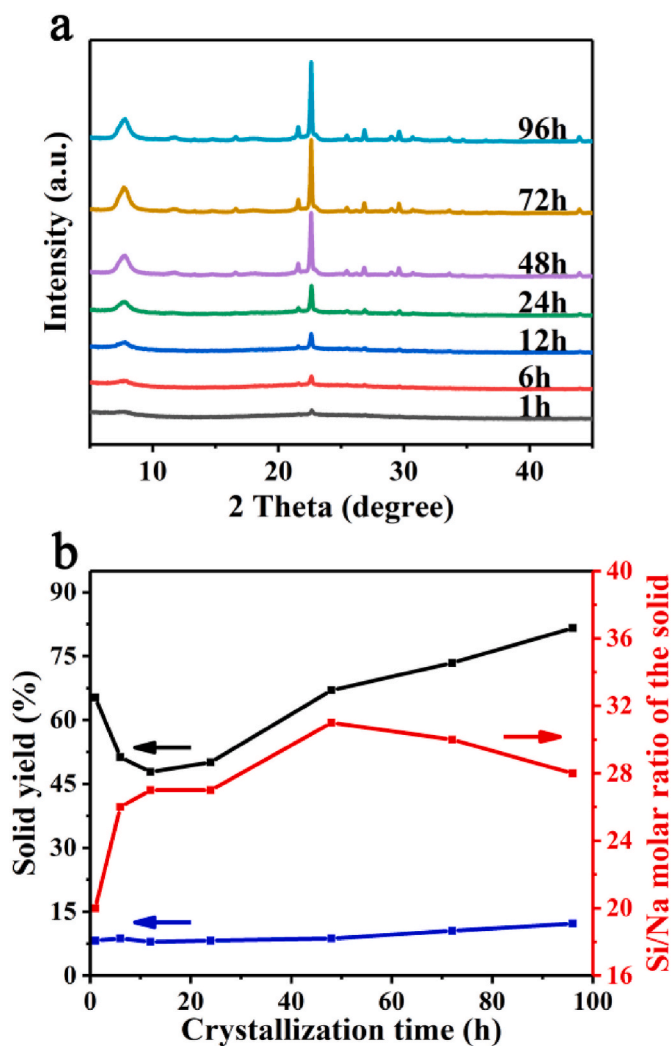


Fig. 2. The evolution of XRD patterns (a), solid yields (black line) and Si/Na molar ratios (b) of siliceous Beta zeolite (sample 5) with different crystallization times. The solid yields of contrast syntheses without the addition of NaCl were also shown in figure b (blue line). (For interpretation of the references to colour in this figure legend, the reader is referred to the Web version of this article.)

zeolite (sample 5) synthesized at  $t = 1$  h, 6 h, 12 h, and 24 h for a more clear view. Meanwhile, the crystallization process of contrast synthesis without the addition of NaCl is also investigated and the results are listed in Fig. 2b, S4 and S5. From Fig. 2a, weak broad peaks assigned to zeolite Beta are observed for the initial 1 h sample, which should result from the added nanoseeds. With the hydrothermal reaction proceeds, the relative crystallinity of the solids presents a gradual increase, which could be confirmed from Fig. S3. After 72 h, the intensity of the XRD pattern reaches its maximum and remains little changed until the end of the crystallization. The solid yield at the initial stage (1 h) is as high as 65.3%, which reduces to 47.8% at 12 h, and then rises slowly to 81.6% at 96 h (Fig. 2b). Clearly, the yields of the whole process of sample 5 are superior to those of contrast syntheses without the addition of NaCl (<12.5% in Fig. 2b). This again demonstrates the importance of NaCl addition on the improvement of solid yield. According to the Si/Na ratios in Fig. 2b, it is supposed that  $\text{Na}^+$  takes part in the initial polymerization of  $\text{SiO}_2$  species and the subsequent crystallization.

The morphology of the solid products is observed by SEM (Fig. 3 and S6). At the initial stage, the solid consists of amorphous materials, in which tiny amounts of spherical Beta nanoseeds may be found. This is consistent with the XRD result. Afterwards, the amount of nanocrystals increases at the expense of amorphous materials. One interesting

phenomenon observed for the 6 h and 12 h samples is that the distribution of nanocrystals in the solids is not homogeneous: some particles mainly consist of nanocrystals, whereas others are amorphous (Fig. S6). It implies that the early Beta crystals may be formed by local solid-solid rearrangement, rather than solution-mediated mechanism. In the latter case, homogeneous distribution of Beta crystals in the solids is expected. As the reaction prolongs, the nanocrystals grow larger, and almost no amorphous materials can be found in the 48 h solid. This implies that the nutrition for crystal growth at the subsequent stage should be mainly from the liquid phase.

The TG-DTA curves of the samples with different crystallization times are displayed in Fig. S7. It is clear that the initial solid contains large amount of OSDA cations comparable to the well-crystallized product. According to the  $\text{N}_2$  sorption isotherms and pore size distribution of the 1 h and 6 h samples (Fig. S8 and Table S2), abundant micropores and mesopores are formed in the initial solids, which are likely owing to the filling of large amounts of OSDA cations. Moreover, the exothermic peaks in the DTA curves are observed to shift towards higher-temperature with the proceeding of crystallization (from 316 °C for 1 h sample to 324 °C for the 48 h sample). This should be related to the increase of structural integrity following the hydrothermal reaction, leading to an incremental difficulty for the removal of OSDA.

Based on the above characterization results, the crystallization process of the siliceous Beta zeolite is proposed as follows (Scheme 1): I) the fast polymerization of liquid-phase  $\text{SiO}_2$  species under the help of  $\text{Na}^+$  and the formation of micro/mesoporous  $\text{SiO}_2$  materials under the assistance of  $\text{TEA}^+$ ; II) the local reorganization on the particle surface of micro/mesoporous  $\text{TEA}^+ \text{-Na}^+ \text{-SiO}_2$  composites; III) the movement of the reorganized hydrogels to the Beta nanoseeds, where surface-induced nucleation occurs and leads to the growth of siliceous Beta crystals; IV) further crystal growth by consuming liquid-phase nutrients, following the complete consumption of amorphous particles.

Regarding the intrinsic reason of the  $\text{Na}^+$  cations inducing the polymerization of  $\text{SiO}_2$  species, it is speculated that the  $\text{SiO}_2$  source dissolving in the alkaline  $\text{Na}^+$ -free solution exists in low degree of polymerization and is negatively charged [46]. The surface of the negative  $\text{SiO}_2$  species would be covered by  $\text{TEA}^+$  cations. The bulky  $\text{TEA}^+$  with symmetric structure inhibits the contact and the polymerization of  $\text{SiO}_2$  species. With the presence of  $\text{Na}^+$ , the  $\text{TEA}^+$  on the surface of  $\text{SiO}_2$  species tends to be partially replaced by  $\text{Na}^+$  cations (higher charge density). Meanwhile, the small size of  $\text{Na}^+$  increases the chance of intimate contact of  $\text{SiO}_2$  species in the liquid, promotes the occurrence of further polymerization and thus contributes to the high solid yield.

### 3.4. Hydrophobicity of siliceous Beta zeolite

The hydrophobicity of siliceous Beta zeolite is important for its application in adsorption, which may influence the adsorption rate, capacity and selectivity of organic compounds [16]. Herein, sample 5 was selected as adsorbent for the investigation. Meanwhile, two samples named  $\text{Ref}_F$  and  $\text{Ref}_{\text{deAl}}$  were prepared as reference adsorbents (Fig. S9).  $\text{Ref}_F$  was synthesized from a fluoride medium with bipyramidal morphology in size of about 3  $\mu\text{m}$ .  $\text{Ref}_{\text{deAl}}$  was obtained by post-synthesis dealumination of aluminosilicate Beta precursor. It consists of spherical nanocrystallites ranging from 80 to 100 nm. Table 2 shows the textural properties of all the samples, which evidence their good crystallinity. It is noted that  $\text{Ref}_{\text{deAl}}$  possesses the largest external surface area (173  $\text{m}^2/\text{g}$ ) and mesoporous volume (0.18  $\text{cm}^3/\text{g}$ ) among the samples, which is consistent with its small crystal size.

FTIR spectra of the samples were measured and the  $\nu(\text{OH})$  vibration region are displayed in Fig. 4a. The absorption around 3740  $\text{cm}^{-1}$  is ascribed to the external Si-OH on the crystal surface. According to the literatures, this band may contain the contribution of internal isolated Si-OH, which generally has absorption around 3730  $\text{cm}^{-1}$ . The broad band in the range of 3330–3650  $\text{cm}^{-1}$  corresponds to the hydrogen-

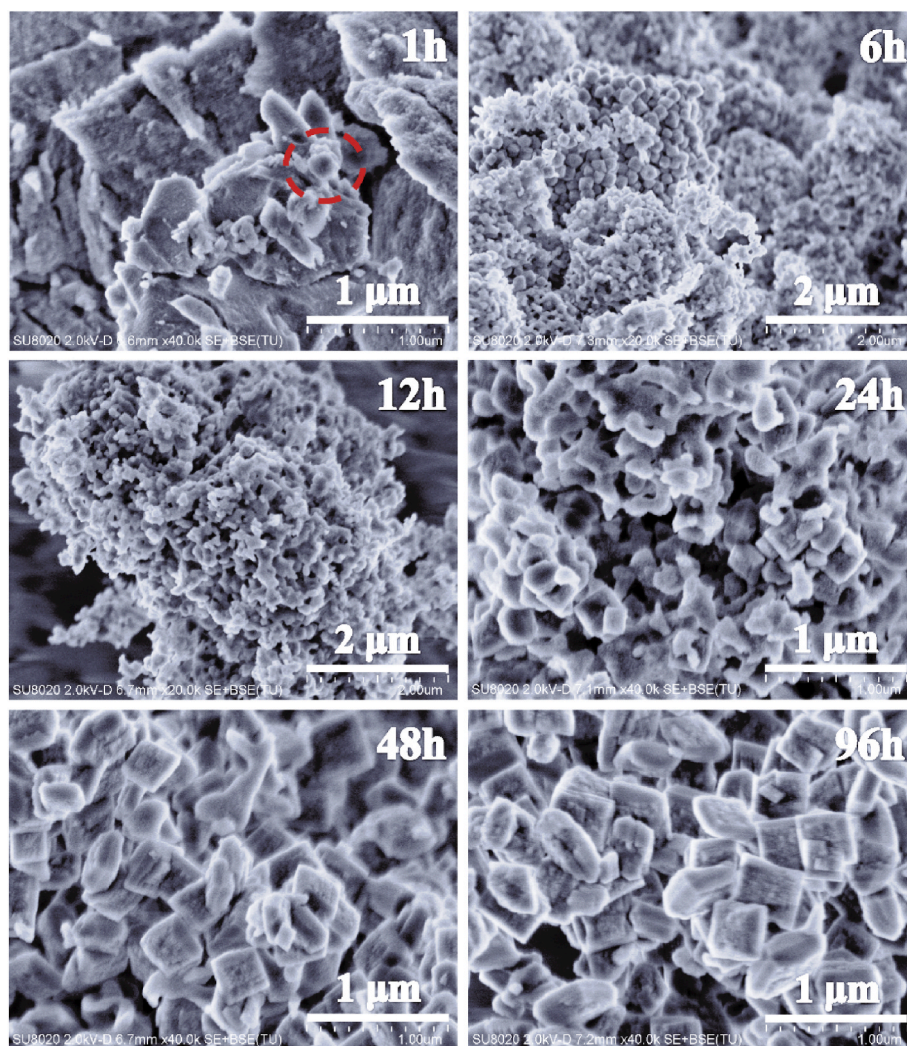
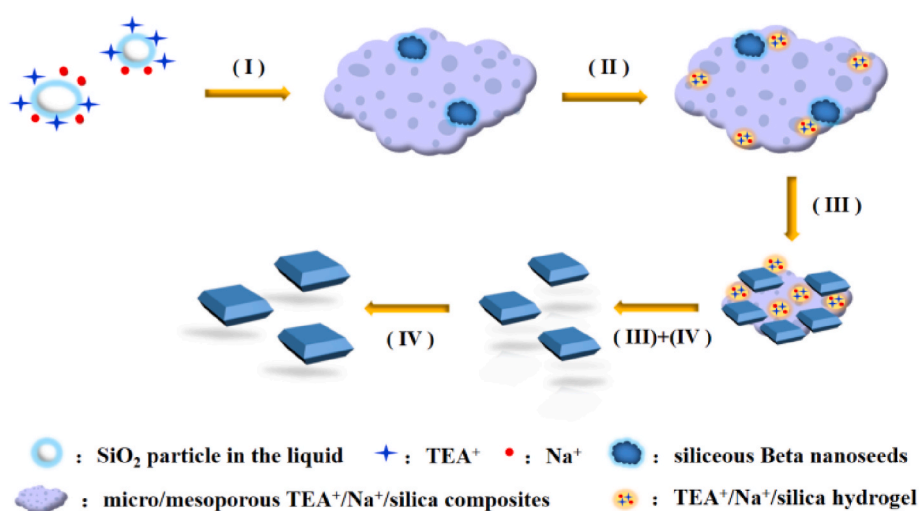


Fig. 3. The SEM images of siliceous Beta zeolites (sample 5) with different crystallization times.



Scheme 1. Proposed crystallization mechanism for siliceous Beta zeolite by fluoride-free hydrothermal synthesis under the assistance of  $\text{Na}^+$  and seeds. The cations adsorbed on the gel/solid surface are omitted for clarity.

bonded Si-OH in the silanol nests [48,49]. Clearly, sample Ref<sub>r</sub> has very weak absorption in the  $\nu(\text{OH})$  vibration region, implying the low amount of Si-OH defects in its framework. This is reasonable as the  $\text{F}^-$  can

balance the charge of OSDA cations and greatly reduce the formation of framework defects. On the contrary, sample Ref<sub>deAl</sub> shows the strongest absorption among the samples, which means the existence of large

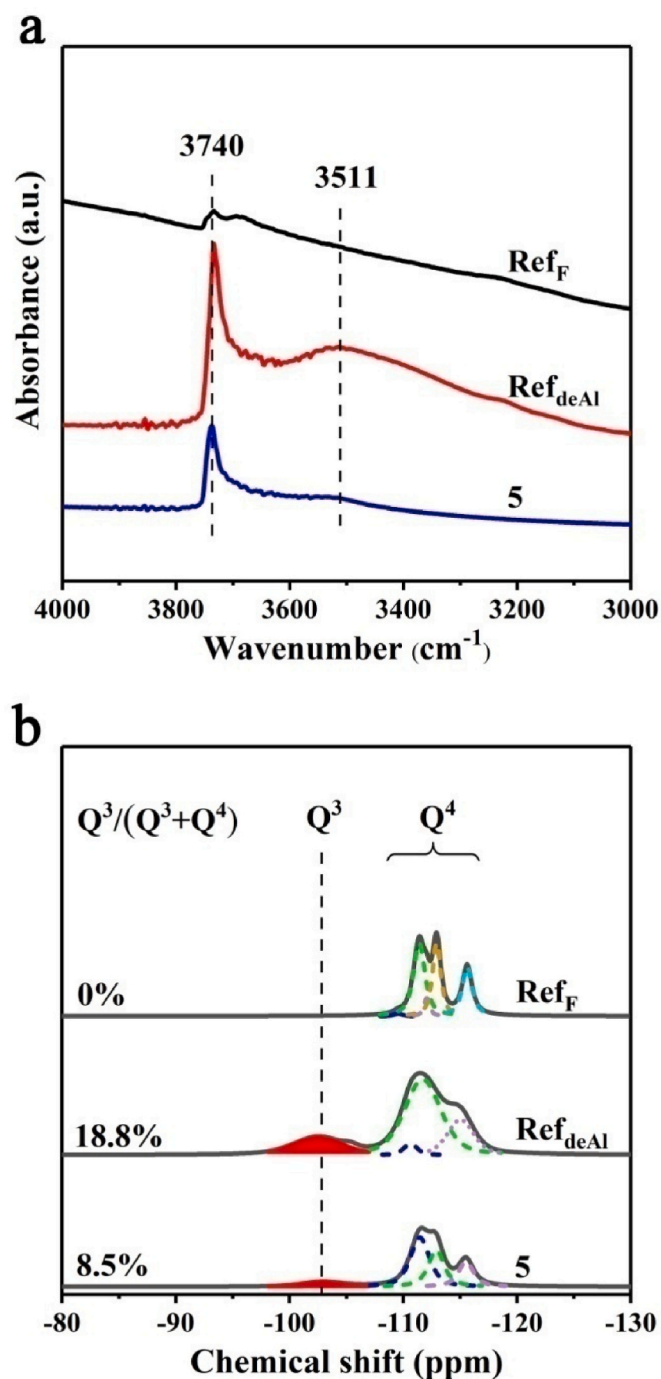


Fig. 4. FTIR spectra in the  $\nu(\text{OH})$  vibration region (a) and  $^{29}\text{Si}$  MAS NMR spectra (b) of siliceous Beta zeolites.

amounts of Si–OH defects generated by dealumination. The intensity of the  $\nu(\text{OH})$  vibration bands on sample 5 is stronger than on  $\text{Ref}_F$ , but obviously lower than on  $\text{Ref}_{\text{deAl}}$ .

The  $^{29}\text{Si}$  MAS NMR spectra of the samples are shown in Fig. 4b. Each spectrum can be deconvoluted into four or five resonances in the region of  $-95$  to  $-120$  ppm. The resonance at  $-102.6$  ppm is ascribed to Si ( $\text{OSi}$ ) $_3(\text{OH})$  groups ( $\text{Q}^3$ ) and the other ones at high field are assigned to Si ( $\text{OSi}$ ) $_4$  groups ( $\text{Q}^4$ ) [44,50]. These assignments are in good consistency with the  $^{29}\text{Si}$  CP MAS NMR spectra, showing an obvious increase in the signal intensity around  $-102$  ppm (Fig. S10). According to the deconvolution results shown in Fig. 4b, the content of  $\text{Q}^3$  species on the samples has the following order:  $\text{Ref}_{\text{deAl}} > \text{sample 5} > \text{Ref}_F$ , which agrees

with the FTIR results.

Water vapor adsorption experiments were carried out to learn the hydrophobicity of the samples. As shown in Fig. 5, sample  $\text{Ref}_F$  gives the lowest water adsorption capacity, suggesting its superior hydrophobicity. The water uptake on sample 5 is larger than on  $\text{Ref}_F$ , but lower than on  $\text{Ref}_{\text{deAl}}$ . On the whole, the distinct hydrophobicity of the samples is in line with the amount of Si–OH defects in the frameworks as revealed by FTIR and  $^{29}\text{Si}$  MAS NMR [51].

### 3.5. VOCs adsorption and breakthrough curves on siliceous Beta zeolites

Adsorption experiments of toluene on siliceous Beta zeolites were conducted to assess their VOCs adsorption performance. Herein, toluene was chosen as a probe molecule, as it is one of the most common VOCs. From Fig. 6, sample 5 shows toluene uptake of 21.7 wt% under the investigated conditions, which is superior to those of sample  $\text{Ref}_F$  (17.3 wt%) and sample  $\text{Ref}_{\text{deAl}}$  (18.4 wt%). Generally, hydrophobicity and pore volume of the adsorbents are the main factors determining the adsorption performance. Zhu et al. [15] once demonstrated that the pore volume of siliceous Beta dominated the adsorption capacity over the hydrophobicity. Therefore, the inferior toluene uptake over sample  $\text{Ref}_F$  may be owing to its relatively low pore volume (Table 2). For sample  $\text{Ref}_{\text{deAl}}$ , its lower toluene uptake, however, is caused by its worst hydrophobicity. The superior adsorption performance over sample 5 should result from a joint contribution of better hydrophobicity and larger pore volume.

Furthermore, breakthrough experiments were carried out to determine the dynamic adsorption capacity of the materials under humid condition, which is more close to the practical application scenarios. As shown in Fig. 7, toluene experienced breakthrough after 52 min on sample 5, obviously longer than that (42 min) on  $\text{Ref}_F$ , meaning that the dynamic toluene adsorption capacity on sample 5 is 24% larger than on  $\text{Ref}_F$ . These preliminary results indicate that the siliceous Beta zeolite synthesized by inorganic cation-driven strategy is promising candidate for the adsorption of VOCs.

## 4. Conclusions

An inorganic cation-driven polymerization strategy has been developed to realize the fluoride-free hydrothermal synthesis of siliceous Beta zeolite. The intrinsic effect of inorganic cations (such as  $\text{Na}^+$ ,  $\text{Li}^+$ , and  $\text{Mg}^{2+}$  etc.) was revealed to be owing to their promoting effect on the polymerization of  $\text{SiO}_2$  species in the liquid synthesis system. The

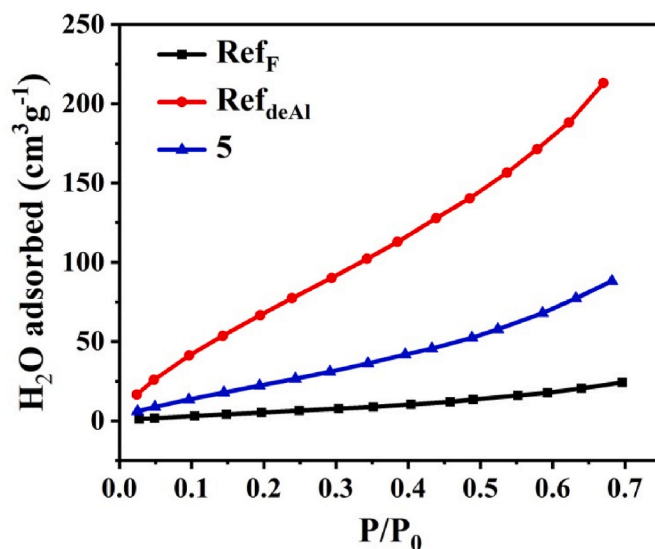


Fig. 5. Water vapor adsorption isotherms of siliceous Beta zeolites (20 °C).

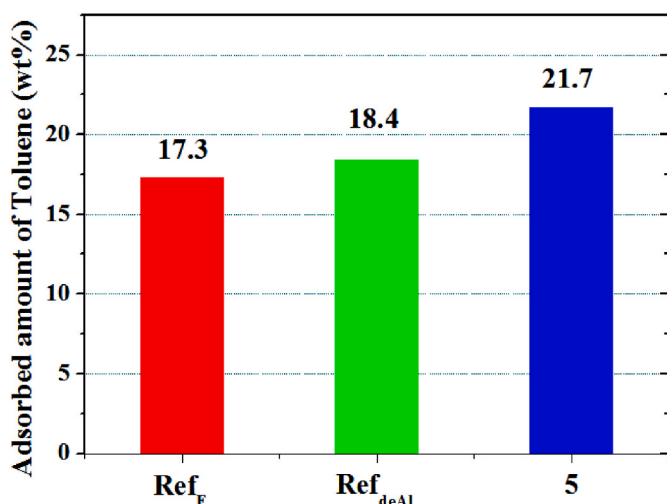


Fig. 6. Adsorption of toluene on siliceous Beta zeolites by IGA (25 °C, P/P<sub>0</sub> = 0.9).

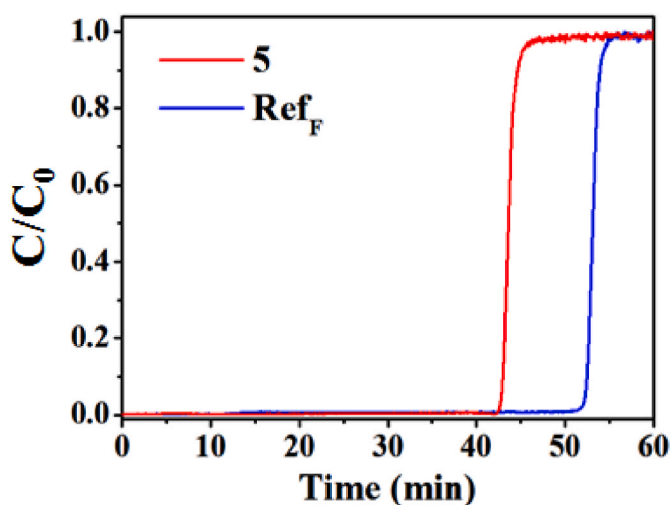


Fig. 7. Breakthrough curves of toluene on siliceous Beta zeolites under humid condition (GHSV = 12000 mL g<sup>-1</sup> h<sup>-1</sup>, P<sub>toluene</sub> = 1.87 kPa, P<sub>H<sub>2</sub>O</sub> = 0.87 kPa, 30 °C).

formation of siliceous Beta follows a solid-solid hydrogel rearrangement mechanism at the initial 48 h. Subsequently, solution-mediated pathway contributes to the further crystal growth. The obtained siliceous Beta has few framework defects, high hydrophobicity and large static adsorption uptake for toluene. More interestingly, the material shows large dynamic toluene adsorption capacity under humid condition, which is 24% higher than that of sample Ref<sub>F</sub> synthesized by fluoride route. It is anticipated that the present synthesis strategy would promote the large-scale production and application of siliceous Beta and facilitate the synthesis of meta-containing Beta and other siliceous zeolites.

#### Declaration of competing interest

The authors declare that they have no known competing financial interests or personal relationships that could have appeared to influence the work reported in this paper.

#### Acknowledgments

The authors acknowledge the National Natural Science Foundation of China (Nos. 21991090 and 21991091) and the Key Research Program

of Frontier Sciences, Chinese Academy of Sciences (Grant No. QYZDB-SSW-JSC040).

#### Appendix A. Supplementary data

Supplementary data to this article can be found online at <https://doi.org/10.1016/j.micromeso.2021.111557>.

#### References

- [1] M.E. Davis, Ordered porous materials for emerging applications, *Nature* 417 (2002) 813–821.
- [2] S. Babel, T.A. Kurniawan, Low-cost adsorbents for heavy metals uptake from contaminated water: a review, *J. Hazard Mater.* 97 (2003) 219–243.
- [3] Y.S. Tao, H. Kanoh, L. Abrams, K. Kaneko, Mesopore-modified zeolites: preparation, characterization, and applications, *Chem. Rev.* 106 (2006) 896–910.
- [4] X.J. Meng, F.S. Xiao, Green routes for synthesis of zeolites, *Chem. Rev.* 114 (2014) 1521–1543.
- [5] M.E. Davis, R.F. Lobo, Zeolite and molecular-sieve synthesis, *Chem. Mater.* 4 (1992) 756–768.
- [6] L. Zhang, Y.X. Peng, J. Zhang, L. Chen, X.J. Meng, F.S. Xiao, Adsorptive and catalytic properties in the removal of volatile organic compounds over zeolite-based materials, *Chin. J. Catal.* 37 (2016) 800–809.
- [7] I. Khalil, K. Thomas, H. Jabraoui, P. Bazin, F. Mauge, Selective elimination of phenol from hydrocarbons by zeolites and silica-based adsorbents-Impact of the textural and acidic properties, *J. Hazard Mater.* 384 (2020) 121397.
- [8] K.J. Kim, H.G. Ahn, The effect of pore structure of zeolite on the adsorption of VOCs and their desorption properties by microwave heating, *Microporous Mesoporous Mater.* 152 (2012) 78–83.
- [9] D.L. Zhu, L.Y. Wang, D. Fan, N.N. Yan, S.J. Huang, S.T. Xu, P. Guo, M. Yang, J. M. Zhang, P. Tian, Z.M. Liu, A bottom-up strategy for the synthesis of highly siliceous faujasite-type zeolite, *Adv. Mater.* 32 (2020) 2000272.
- [10] F.I. Khan, A.K. Ghoshal, Removal of volatile organic compounds from polluted air, *J. Loss Prev. Process. Ind.* 13 (2000) 527–545.
- [11] R. Otomo, T. Yokoi, T. Tatsumi, Synthesis of isosorbide from sorbitol in water over high-silica aluminosilicate zeolites, *Appl. Catal. A-Gen.* 505 (2015) 28–35.
- [12] H. Yang, P.P. Yang, X.H. Liu, Y.Q. Wang, Space-confined synthesis of zeolite Beta microspheres via steam-assisted crystallization, *Chem. Eng. J.* 299 (2016) 112–119.
- [13] J.L. Zhang, P. Cao, H.Y. Yan, Z.J. Wu, T. Dou, Synthesis of hierarchical zeolite Beta with low organic template content via the steam-assisted conversion method, *Chem. Eng. J.* 291 (2016) 82–93.
- [14] J. Stelzer, M. Paulus, M. Hunger, J. Weitkamp, Hydrophobic properties of all-silica zeolite beta, *Microporous Mesoporous Mater.* 22 (1998) 1–8.
- [15] Z.G. Zhu, H. Xu, J.G. Jiang, H.H. Wu, P. Wu, Hydrophobic nanosized all-silica beta zeolite: efficient synthesis and adsorption application, *ACS Appl. Mater. Interfaces* 9 (2017) 27273–27283.
- [16] M. Van den Bergh, A. Krajnc, S. Voorspoels, S.R. Tavares, S. Mullens, I. Beurroies, G. Maurin, G. Mali, D.E. De Vos, Highly selective removal of perfluorinated contaminants by adsorption on all-silica zeolite beta, *Angew. Chem. Int. Ed.* 59 (2020) 14086–14090.
- [17] T. Ikuno, W. Chaikittisilp, Z.D. Liu, T. Iida, Y. Yanaba, T. Yoshikawa, S. Kohara, T. Wakihara, T. Okubo, Structure-directing behaviors of tetraethylammonium cations toward zeolite beta revealed by the evolution of aluminosilicate species formed during the crystallization process, *J. Am. Chem. Soc.* 137 (2015) 14533–14544.
- [18] M.B. Park, S.H. Ahn, C.P. Nicholas, G.J. Lewis, S.B. Hong, Charge density mismatch synthesis of zeolite beta in the presence of tetraethylammonium, tetramethylammonium, and sodium ions: influence of tetraethylammonium decomposition, *Microporous Mesoporous Mater.* 240 (2017) 159–168.
- [19] V. Valtchev, G. Majano, S. Mintova, J. Perez-Ramirez, Tailored crystalline microporous materials by post-synthesis modification, *Chem. Soc. Rev.* 42 (2013) 263–290.
- [20] Q.Y. Wang, S.T. Xu, J.R. Chen, Y.X. Wei, J.Z. Li, D. Fan, Z.X. Yu, Y. Qi, Y.L. He, S. L. Xu, C.Y. Yuan, Y. Zhou, J.B. Wang, M.Z. Zhang, B.L. Su, Z.M. Liu, Synthesis of mesoporous ZSM-5 catalysts using different mesogenous templates and their application in methanol conversion for enhanced catalyst lifespan, *RSC Adv.* 4 (2014) 21479–21491.
- [21] J.C. Vanderwaal, M.S. Rigutto, H. Vanbekkum, Synthesis OF all-silica zeolite-beta, *J. Chem. Soc., Chem. Commun.* (1994) 1241–1242.
- [22] M.A. Cambor, M. Costantini, A. Corma, L. Gilbert, P. Esteve, A. Martinez, S. Valencia, Synthesis and catalytic activity of aluminium-free zeolite Ti-beta oxidation catalysts, *Chem. Commun.* (1996) 1339–1340.
- [23] R. Mostowicz, F. Testa, F. Crea, R. Aiello, A. Fonseca, J.B. Nagy, Synthesis of zeolite beta in presence of fluorides: influence of alkali cations, *Zeolites* 18 (1997) 308–324.
- [24] Y.C. Cui, Z. Yan, M.L. Li, J. Zhu, L.F. Zhu, H. Yao, X.B. Cao, Solvent-free synthesis of all silica beta zeolite in the presence of tetraethylammonium bromide, *Crystals* 8 (2018) 73.
- [25] Y. Kubota, T. Honda, J. Plevert, T. Yamashita, T. Okubo, Y. Sugi, Synthesis of a new molecular sieve using DABCO-based structure-directing agent, *Catal. Today* 74 (2002) 271–279.

- [26] A. Corma, M.T. Navarro, F. Rey, S. Valencia, Synthesis of pure polymorph C of Beta zeolite in a fluoride-free system, *Chem. Commun.* (2001) 1486–1487.
- [27] M.A. Cambor, A. Corma, S. Valencia, Spontaneous nucleation and growth of pure silica zeolite-beta free of connectivity defects, *Chem. Commun.* (1996) 2365–2366.
- [28] V. Vattipalli, A.M. Paracha, W.G. Hu, H.Y. Chen, W. Fan, Broadening the scope for fluoride-free synthesis of siliceous zeolites, *Angew. Chem. Int. Ed.* 57 (2018) 3607–3611.
- [29] A. Corma, L.T. Nemeth, M. Renz, S. Valencia, Sn-zeolite beta as a heterogeneous chemoselective catalyst for Baeyer-Villiger oxidations, *Nature* 412 (2001) 423–425.
- [30] D. Padovan, L. Botti, C. Hammond, Active site hydration governs the stability of Sn-beta during continuous glucose conversion, *ACS Catal.* 8 (2018) 7131–7140.
- [31] X.M. Yang, L.Y. Wang, T.L. Lu, B.B. Gao, Y.L. Su, L.P. Zhou, Seed-assisted hydrothermal synthesis of Sn-Beta for conversion of glucose to methyl lactate: effects of the H<sub>2</sub>O amount in the gel and crystallization time, *Catalysis Science & Technology* 10 (2020) 8437–8444.
- [32] J.D. Lewis, S. Van de Vyver, Y. Roman-Leshkov, Acid-base Pairs in Lewis acidic zeolites promote direct aldol reactions by soft enolization, *Angew. Chem. Int. Ed.* 54 (2015) 9835–9838.
- [33] H.P. Winoto, Z.A. Fikri, J.M. Ha, Y.K. Park, H. Lee, D.J. Suh, J. Jae, Heteropolyacid supported on Zr-Beta zeolite as an active catalyst for one-pot transformation of furfural to gamma-valerolactone, *Appl. Catal. B Environ.* 241 (2019) 588–597.
- [34] B. Tang, W.L. Dai, X.M. Sun, N.J. Guan, L.D. Li, M. Hunger, A procedure for the preparation of Ti-Beta zeolites for catalytic epoxidation with hydrogen peroxide, *Green Chem.* 16 (2014) 2281–2291.
- [35] D. Lin, Q.D. Zhang, Z.X. Qin, Q. Li, X. Feng, Z.N. Song, Z.P. Cai, Y.B. Liu, X.B. Chen, D. Chen, S. Mintova, C.H. Yang, Reversing titanium oligomer formation towards high-efficiency and green synthesis of titanium-containing molecular sieves, *Angew. Chem. Int. Ed.* 60 (2021) 3443–3448.
- [36] H. Xu, X.D. Wang, P. Ji, H.H. Wu, Y.J. Guan, P. Wu, Hydrothermal synthesis of Sn-Beta zeolites in F<sup>-</sup>-free medium, *Inorg. Chem. Front.* 5 (2018) 2763–2771.
- [37] X.B. Zhao, L.Y. Wang, J.Z. Li, S.T. Xu, W.N. Zhang, Y.X. Wei, X.W. Guo, P. Tian, Z. M. Liu, Investigation of methanol conversion over high-Si beta zeolites and the reaction mechanism of their high propene selectivity, *Catalysis Science & Technology* 7 (2017) 5882–5892.
- [38] R. Li, N. Linares, J.G. Sutjianto, A. Chawla, J. Garcia-Martinez, J.D. Rimer, Ultrasmall Zeolite crystals prepared from highly interdispersed alkali-silicate precursors, *Angew. Chem. Int. Ed.* 57 (2018) 11283–11288.
- [39] K. Cho, K. Na, J. Kim, O. Terasaki, R. Ryoo, Zeolite synthesis using hierarchical structure-directing surfactants: retaining porous structure of initial synthesis gel and precursors, *Chem. Mater.* 24 (2012) 2733–2738.
- [40] M. Manko, J. Vittenet, J. Rodriguez, D. Cot, J. Mendret, S. Brosillon, W. Makowski, A. Galarneau, Synthesis of binderless zeolite aggregates (SOD, LTA, FAU) beads of 10, 70 μm and 1 mm by direct pseudomorphic transformation, *Microporous Mesoporous Mater.* 176 (2013) 145–154.
- [41] J.M. Newsam, M.M.J. Treacy, W.T. Koetsier, C.B. Degruyter, Structural characterization of zeolite-beta, *Proc. R. Soc. London Ser. A-Math. Phys. Eng. Sci.* 420 (1988) 375–405.
- [42] T.T. Lu, P. Gao, J. Xu, Y.R. Wang, W.F. Yan, J.H. Yu, F. Deng, X.H. Mu, R.R. Xu, Influence of Al<sup>3+</sup> on polymorph A enrichment in the crystallization of beta zeolite, *Chin. J. Catal.* 36 (2015) 889–896.
- [43] X.W. Cheng, J.J. Mao, X.C. Lv, T. Hua, X.P. Cheng, Y.C. Long, Y. Tang, Fast synthesis of nanosized zeolite beta from a low-seeded, low-templated dry gel with a seeding-steam-assisted conversion method, *J. Mater. Chem.* 2 (2014) 1247–1251.
- [44] A. Vjunov, M.A. Derewinski, J.L. Fulton, D.M. Camaioni, J.A. Lercher, Impact of zeolite aging in hot liquid water on activity for acid-catalyzed dehydration of alcohols, *J. Am. Chem. Soc.* 137 (2015) 10374–10382.
- [45] A. Corma, M.E. Domine, L. Nemeth, S. Valencia, Al-free Sn-beta zeolite as a catalyst for the selective reduction of carbonyl compounds (Meerwein-Ponndorf-Verley reaction), *J. Am. Chem. Soc.* 124 (2002) 3194–3195.
- [46] N.D. Hould, A. Foster, R.F. Lobo, Zeolite beta mechanisms of nucleation and growth, *Microporous Mesoporous Mater.* 142 (2011) 104–115.
- [47] M. Matsukata, T. Osaki, M. Ogura, E. Kikuchi, Crystallization behavior of zeolite beta during steam-assisted crystallization of dry gel, *Microporous Mesoporous Mater.* 56 (2002) 1–10.
- [48] C.C. Chang, H.J. Cho, Z.P. Wang, X.T. Wang, W. Fan, Fluoride-free synthesis of a Sn-BEA catalyst by dry gel conversion, *Green Chem.* 17 (2015) 2943–2951.
- [49] P. Li, G.Q. Liu, H.H. Wu, Y.M. Liu, J.G. Jiang, P. Wu, Postsynthesis and selective oxidation properties of nanosized Sn-beta zeolite, *J. Phys. Chem. C* 115 (2011) 3663–3670.
- [50] O. Larlus, V. Valtchev, Synthesis of all-silica BEA-type material in basic media, *Microporous Mesoporous Mater.* 93 (2006) 55–61.
- [51] P. Wolf, M. Valla, F. Nunez-Zarur, A. Comas-Vives, A.J. Rossini, C. Firth, H. Kallas, A. Lesage, L. Emsley, C. Coperet, I. Hermans, Correlating synthetic methods, morphology, atomic-level structure, and catalytic activity of Sn-beta catalysts, *ACS Catal.* 6 (2016) 4047–4063.